



INFLUENCE OF HIGH STRENGTH REINFORCING STEEL ON SEISMIC PERFORMANCE OF CONCRETE SPECIAL MOMENT FRAMES

K. Zhong⁽¹⁾, G. G. Deierlein⁽²⁾

⁽¹⁾ Ph.D. student, Department of Civil and Environmental Engineering, Stanford University, kuanshi@stanford.edu

⁽²⁾ John A. Blume Professor, Department of Civil and Environmental Engineering, Stanford University, ggd@stanford.edu

Abstract

The new US concrete building design code (ACI 318-19) starts to permit the use of Grade 80 steel as the longitudinal reinforcement in special moment frames (SMF). Meanwhile, it includes the extra requirements on minimum reinforcement tensile-to-yield strength ratio (T/Y), minimum fracture elongation, and maximum transverse reinforcement spacing ratio (s/d_b) to ensure the sufficient strain hardening and ductility under large earthquakes. These requirements are built on concerns about potential reinforcement fatigue and fracture as well as the subsequent implications on the system-level seismic performance.

To help rationalize these requirements and build more confidence of utilizing high-strength reinforcement (yield strength greater than 60 ksi or 400 MPa) in general, this paper introduces the findings of the study of evaluating the influence of high-strength reinforcement on the seismic performance of concrete SMF. First, a parametric fatigue-fracture model is developed to capture reinforcement failures observed in the available bare-bar experimental data. The model uses the fracture index (FI) to represent the fatigue-fracture damage, which captures the following trends: (1) rebars with higher yield strength (f_y) are found to have relatively lower fracture-fatigue resistance; (2) larger slenderness ratios are found to cause significant strain localizations after rebar buckling, which in turn reduce the fatigue resistance; and (3) rebars with higher T/Y have larger fracture resistance under large-strain cycles. Second, a comparative assessment is conducted for 27 archetype designs of one 20-story SMF: (1) incremental dynamic analysis (IDA) with calibrated concentrated hinge models are performed in OpenSees; (2) detailed fiber-based models of beams and columns are analyzed under deformation histories from IDA to estimate rebar cyclic strain demands; and (3) reinforcement fracture is quantified by the parametric model as a non-simulated failure mode in FEMA P-695. To evaluate the overall influence of high-strength reinforcing steel on the seismic performance of concrete SMF, comparisons are made among archetype designs on (1) rebar fracture risks and (2) collapse risks including fracture-induced failure modes. It is found that the rebar fracture and structural collapse risk can be reduced by increasing T/Y and decreasing s/d_b . Provided the corresponding requirements in the ACI 318-19, the bar fracture risks and collapse risks of the archetype frames with Grade 80 reinforcement are comparable to conventional frames with Grade 60 reinforcement (yield strength of 400 MPa). Meanwhile, if conform to the same requirements, the archetype frames using Grade 100 reinforcement also have the acceptable collapse safety at MCE_R .

Keywords: high-strength reinforcement; fatigue; fracture; collapse safety; concrete special moment frame



1. Introduction

In response to the increasing interest from industry, the National Institute of Standards and Technology (NIST) and the Applied Technology Council (ATC) initiated the project ATC-98 evaluating the use of high-strength reinforcement (yield strength greater than 60 ksi or 400 MPa) as primary reinforcement in seismic applications [1]. The Charles Pankow Foundation (CPF) funded the project ATC-115 [2] identifying research needs and milestones for incorporating high-strength longitudinal reinforcement in seismic design standards. One major concern with high-strength reinforcement is whether it has the sufficient strain hardening and ductility to resist fracture under inelastic cyclic loading that may occur in buildings subjected to large earthquakes.

In order to characterize the fatigue and fracture resistance of high-strength reinforcement, bare-bar tests were conducted under the standard monotonic tensile and various constant-amplitude cyclic loading protocols [3]. Two major manufacturing processes were examined in these tests: (1) quenching and tempering and (2) micro-alloying. In the low-cycle fatigue experiments, three different bar slenderness ratios (i.e., 4, 5, and 6) were used to quantify the buckling impacts on the fatigue life. On average, it was found that Grade 80 and Grade 100 reinforcement have relatively lower fracture and fatigue resistances than Grade 60 reinforcement. Meanwhile, large variations were seen in tested strain lives of high-strength reinforcement. In order to investigate the ductility of concrete beam-column members with Grade 100 longitudinal reinforcement, pseudo-static experiments were conducted under standard cyclic loading protocols [4, 5]. Compared to the benchmark specimen using Grade 60 bars, the specimens with Grade 100 bars had similar lateral drift capacities, but the strain demands of Grade 100 reinforcement were found to be higher due to the reduced plastic hinge length. Subject to the combined effects of lower fatigue resistances and higher strain demands, Grade 100 bars ruptured earlier in tests.

Balancing the benefits of high-strength reinforcement (e.g., cost-efficiency and constructability) and the design strategies of preventing premature bar fractures, the new ACI 318-19 Building Code [6] permits the use of Grade 80 steel for longitudinal reinforcement in special moment frames but requires reinforcing steel to have a minimum tensile-to-yield strength ratio (T/Y) of 1.25 and a minimum fracture elongation based on bar diameters. Meanwhile, the maximum transverse reinforcement spacing ratio (s/d_b) is reduced to 5.0 to alleviate bar buckling impacts.

To help rationalize these requirements and build more confidence in utilizing higher grade reinforcement (Grade 100), this paper introduces a systematical study on evaluating the influence of high-strength reinforcement on seismic performance of concrete special moment frames by following steps. First, a new parametric model is developed and calibrated to capture the observed fatigue-fracture characteristics of high-strength reinforcement in the aforementioned bare-bar experiments. Second, a new approach for determining the hinge properties of the concentrated IMK hinge model [7] is developed especially to better simulate the cyclic responses of concrete framing members using high-strength reinforcement. Utilizing the calibrated concentrated hinge model, overall 27 different frames are idealized to 2D models in OpenSees [8]. The incremental dynamic analysis (IDA) [9] is conducted for each archetype frame. The detailed fiber-element analysis is performed to simulate the steel strain histories in critical framing elements, based on which the maximum fracture index in the building is evaluated by the proposed parametric model. Extending FEMA P-695 methodology [10], the reinforcement fracture is considered as a non-simulated failure mode in collapse assessment. Last but not least, the maximum fracture index demands as well as the collapse fragilities of different designs are contrasted to demonstrate the influence from steel grade (f_y), T/Y , and s/d_b on the seismic performance of concrete special moment frames using high-strength reinforcement.

2. Parametric Reinforcement Fatigue-Fracture Model

Although the literature about material fatigue can be traced back to roughly a century ago, most fatigue models used for engineering applications are inherently empirical. The cyclic fatigue life under elastic



cycles was first found to be dependent on stress amplitude [11]. Then, the concept that cyclic fatigue life relies on strain range (strain-based model) was concluded by Manson [12] to predict fractures under inelastic cycles, where the stress range is not a reliable measure in cyclic strain-hardening/softening materials. The strain-based model is built on the hypothesis that the plastic strains are proportional to the irreversible damage in a log-log linear manner. The accuracy of Manson's original model has been verified and improved by many investigations [13, 14] for the low-cycle fatigue problems whose half-cycle number ranges from 100 to 10^3 . More recently, the strain-based model was also applied to constant-amplitude cyclic tests of bare reinforcement [3, 15, 16] with the highlighted observations: (1) the half-cycle number before bar rupture decreases as the plastic strain range increases; (2) for a specific reinforcing steel material, a log-log linear function between N_f and ε_p with 2 material-dependent parameters can be fitted to the observed trend; (3) the mean stress and strain have negligible effect on fatigue life under cycles with strain amplitudes larger than 1%; (4) the reinforcement buckling leads to strain localizations, which in turn reduce the fatigue life; and (5) the average fatigue lives of Grade 80 and Grade 100 reinforcement are shorter than the average fatigue life of Grade 60 reinforcement.

Corresponding to these observations, a parametric reinforcement fatigue-fracture model is developed to address three major issues: (1) calibrating the general fatigue-fracture model to represent the unique failure mechanisms of different reinforcing bars; (2) differentiating cyclic fatigue/fracture resistances of different reinforcing bars based on measurable material properties; and (3) relating the bar fatigue resistance to the bar slenderness (s/d_b).

The parametric model is adapted from the classical Coffin-Manson model shown in Eq. (1), which relates the cyclic plastic strain amplitude, ε_p , to the number of cycles at fracture, N_f , through an exponential expression. Three material parameters (α_f , C_f , and ε_f) are calibrated for overall 32 independent test groups of various steel grades, steel manufacturing processes, or bar slenderness ratios (based on overall 206 individual bar tests [5]). As indicated by the illustrative calibrations in Fig. 1, the fatigue resistance is negatively correlated with f_y and s/d_b . Meanwhile, the fatigue resistance is also positively correlated with T/Y under large strain cycles but negatively correlated with T/Y under small strain cycles. Based on these calibrated models and measured steel property data, linear regressions are conducted to find the predictive equations for the three material parameters, as expressed in Eq. (2). Fig. 2a and 2b show the comparisons between the calibrated and predicted values of α_f and C_f .

$$\varepsilon_p = C_f (2N_f)^{-\alpha_f} \quad (1)$$

$$\begin{cases} \alpha_f = 0.080 - 0.045 \cdot (f_y/60\text{ksi}) + 0.027 \cdot (s/d_b) + 0.129 \cdot (T/Y) \\ C_f = 0.5^{\alpha_f} \cdot (\varepsilon_f - f_y/E_s) \\ \varepsilon_f = f_y/E_s - 0.043 \cdot (f_y/60\text{ksi}) + 0.128 \cdot (T/Y) + 0.018 \cdot (d_b/\text{lin}) \end{cases} \quad (2)$$

where, f_y is yield strength; E_s is Young's modulus; T/Y is tensile-to-yield strength ratio; d_b is bar diameter; s/d_b is bar slenderness; and ε_f is fracture elongation (over 8-inch gauge length).

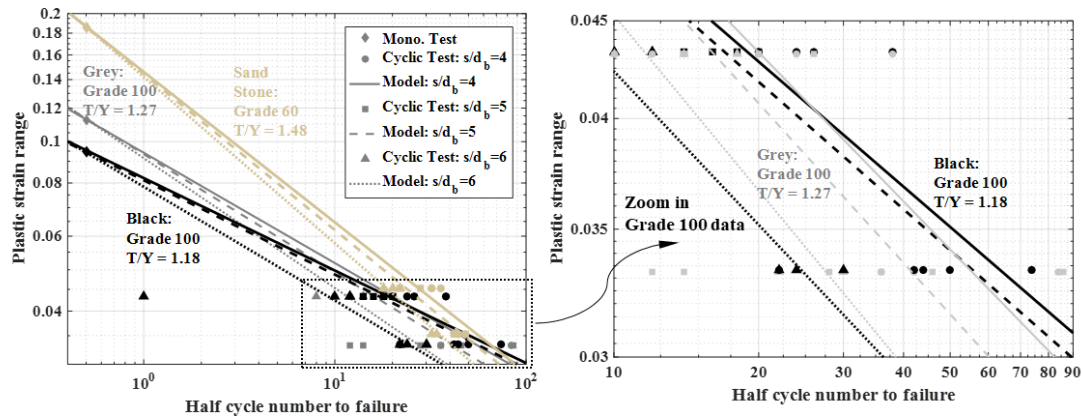


Fig. 1 - Example of calibrated models versus test data for #8 Grade 60 and Grade 100 reinforcement. (Note: reinforcement grades represent specified yield strength in ksi; 1.00 ksi = 6.89 MPa.)

Following the Miner's Rule [11] and the rain-flow counting algorithm [17], the parametric model is formulated in Eq. (3), which is a function of the plastic strain amplitudes and the material parameters.

$$FI = \sum_{i=1}^N (\varepsilon_{pi} / C_f)^{1/\alpha_f} \quad (3)$$

where, ε_{pi} is the plastic strain amplitude of i^{th} half cycle based the rain-flow counting method; and N is total number of counted half cycles. The fracture index (FI) is defined as a damage measure for reinforcement fracture under random loading protocols. The FI is back-calculated for each test group by substituting (1) the calibrated material parameters, (2) the strain-amplitude, and (3) the average half-cycle number into Eq. (3). Fig. 2c shows the cumulative distribution of back-calculated fracture indices, which follow the lognormal cumulative distribution (fragility) function with median of 1.0 and dispersion of 0.5.

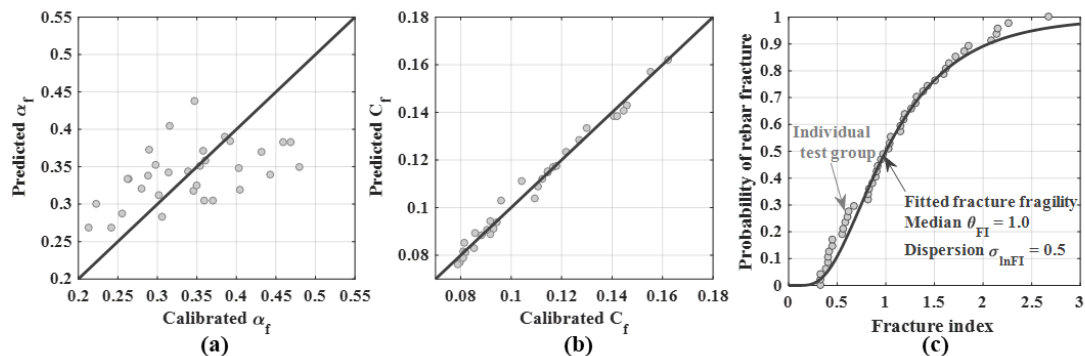


Fig. 2 - The cumulative distribution (fragility) function of fracture indices at bar fracture failure.

Detailed fiber-based beam-column models (Fig. 3a) are built in OpenSees [8] to further examine whether this new parametric fatigue-fracture model could capture bar ruptures that are observed in concrete member experiments (Fig. 3b). Overall 12 CPF reinforced concrete subassembly tests are used in this validation (i.e., 4 beam tests by To and Moehle [4]; 4 column tests by Sokoli et al. [5]; and 4 T-shape wall tests by Huq et al. [18]). For each test, the fiber element model is analyzed under the test loading protocol. The measured reinforcement material properties are used in Eq. (2) to predict the material parameters. The simulated reinforcing steel strain at the base section is used in Eq. (3) to compute the FI history of each experiment. As shown in Fig. 4a, for every beam/column test, two FI histories are traced for both top and bottom bars in the section. For every T-shape wall test, the FI history of the bottom bar in the stem is focused. In experiments without bar rupture, the FI_{max} is taken as the FI at the end of the loading protocol; whereas, in experiments with bar rupture(s), the FI_{max} is the FI at the end of the half cycle having the first bar



fracture in the corresponding direction. Fig. 4b compares the computed FI_{max} values of these 12 tests, where the average FI_{max} is 1.15 for tests having bar ruptures, and the average FI_{max} is 0.70 for tests that did not have bar fracture failure. Although the result might be slightly conservative, the developed fatigue-fracture model is deemed to predict the bar fracture by $FI_{max} = 1.0$, given the good agreement in these validation results. Details of the validation study can be found in the authors' report [19].

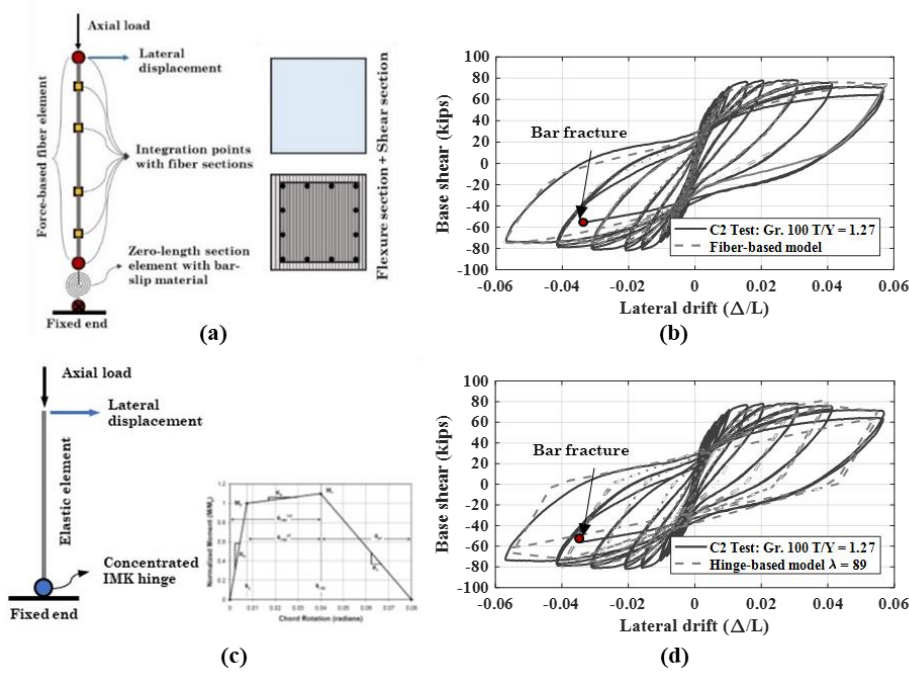


Fig. 3 - Test data versus simulated responses of the high-strength steel reinforced specimen [6]: (a) fiber-based model approach; (b) hysteresis comparison with fiber-based model; (c) Hinge-based model approach; (d) hysteresis comparison with hinge-based model. (Note: 1.00 kip = 4.45 kN.)

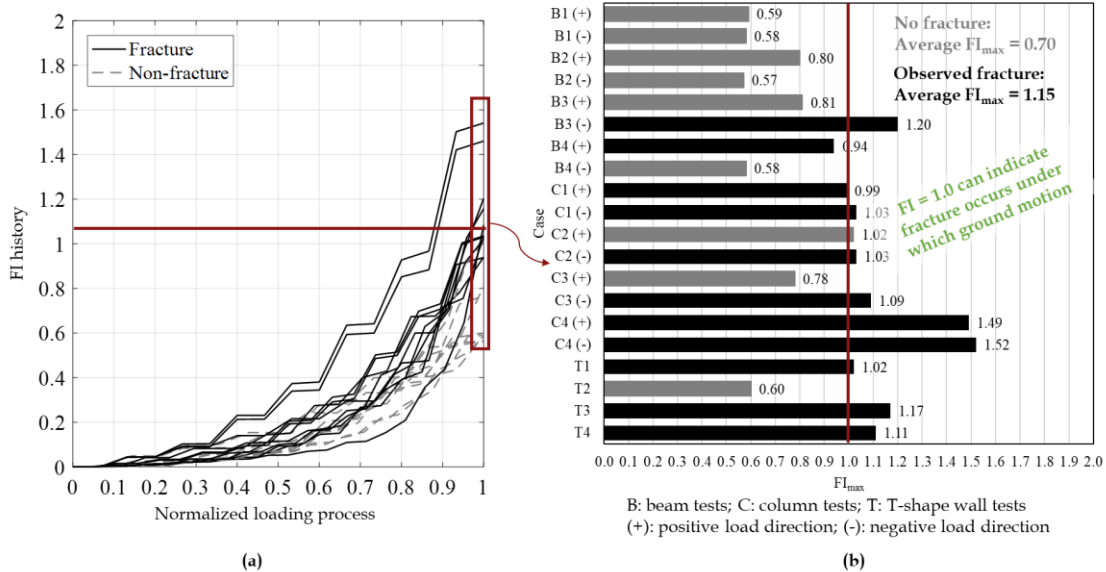


Fig. 4 - Validation of the proposed reinforcement fatigue-fracture model in subassembly tests. (a) FI histories under the normalized loading process. (b) FI_{max} .



3. Reinforced Concrete Beam-Column Hinge Model

The IMK model [7] is commonly used to simulate cyclic responses of concrete framing members with explicitly modeled cyclic deteriorations (Fig. 3c). The predictive equations for 6 hinge properties have been developed and used in previous researches to assess the seismic performance of reinforced concrete moment frames [20, 21]. However, given the different yielding and hardening behaviors observed in recent tests [4, 5], these modeling parameters should be re-calibrated to reliably simulate the cyclic behaviors of high-strength steel reinforced concrete members. In this study, the 5 backbone-curve parameters of the IMK model (M_y , θ_y , M_c , θ_{cap} , and θ_{pc}) are determined by performing the fiber-based cross-section analysis and aggregating shear and bar-slip relations to obtain the overall M - θ relation. Hence, the steel yield stress, tensile-to-yield strength ratio, and uniform strain are explicitly considered in the hinge properties. Meanwhile, the cyclic deterioration factor of the IMK model (λ) is re-calibrated to a data set including 104 beam-column tests to best capture the cyclic strength and stiffness deterioration due to bar buckling [19]. Based on the calibrated results, a new predictive equation for λ is developed, as shown in Eq. (4).

$$\lambda = (253.09)(0.17)^{\nu} (0.92)^{L/h} (1.10)^{T/Y} (1.38)^{\rho_{sh,eff}} (0.94)^{s_n} \quad (4)$$

where, ν is axial load ratio; L/h is the shear span ratio; $\rho_{sh,eff}$ is effective transverse reinforcement ratio, i.e., $\rho_{sh,eff} = A_{sh}f_y/(bsf_c')$ where A_{sh} is transverse reinforcement area, b is section width, s is tie spacing; and s_n is effective bar slenderness, $s_n = (s/d_b)(f_y/100 \text{ Mpa})^{0.5}$. Fig. 5 shows the comparison between the predicted and calibrated values of λ for the collected data set. It is highlighted that the new predictive equation has a good agreement with the recent CPF beam and column tests using high strength reinforcement [5, 6]. Utilizing the concentrated hinge model, Fig. 3d shows the simulated cyclic responses of the C2 column specimen which closely fit the test data [6].

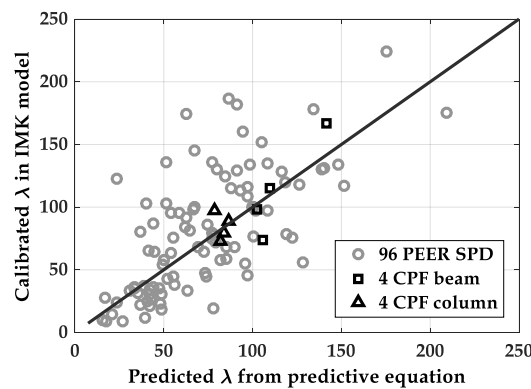


Fig. 5 - Comparison: predicted λ vs. calibrated λ .

4. Seismic Performance Assessment Framework

In FEMA P-695 [10], the seismic performance is assessed by nonlinear structural analysis under incrementally scaled ground motions until collapse. The median collapse intensity is adjusted by a spectral shape factor (SSF) based on seismic hazard characteristics and structural period and ductility; and the dispersion is determined to account for uncertainties associated with ground motions, structural modeling, implementation of design intent, and uncertainties in structural behaviors.

In terms of incorporating the extra collapse risk due to reinforcement fracture, this study extends the concept of non-simulated collapse mode (NSC) in FEMA P-695 [10]. Fig. 6 illustrate the major steps of this framework. It starts with the IDA of the frame model. In every time history analysis, in addition to the maximum story drift ratio (SDR_{max}), the lateral drift history of each framing element is also recorded. Detailed fiber-based model is then built for each framing member and analyzed under the corresponding lateral drift history from the frame analysis. Based on the fiber-based analysis, the simulated reinforcing bar



strain history at the most critical location (usually at the end integration point) is used in the parametric reinforcement fatigue-fracture model to compute the fracture index. Following this procedure, the maximum fracture index (FI_{max}) in the building can be determined in each time history analysis. Finally, as suggested by FEMA P-695 [10] that the non-simulated fracture failure can be incorporated by adjusting the IDA results with additional limits on corresponding demand parameters, the fracture-induced collapse is assumed to occur on the set of the FI_{max} exceeding 1.0 which is a relatively conservative limit for the fracture-induced collapse. In other words, the collapse intensity under a ground motion is the smaller of the intensity of the $SDR_{max} = 10\%$ and the intensity of the $FI_{max} = 1.0$.

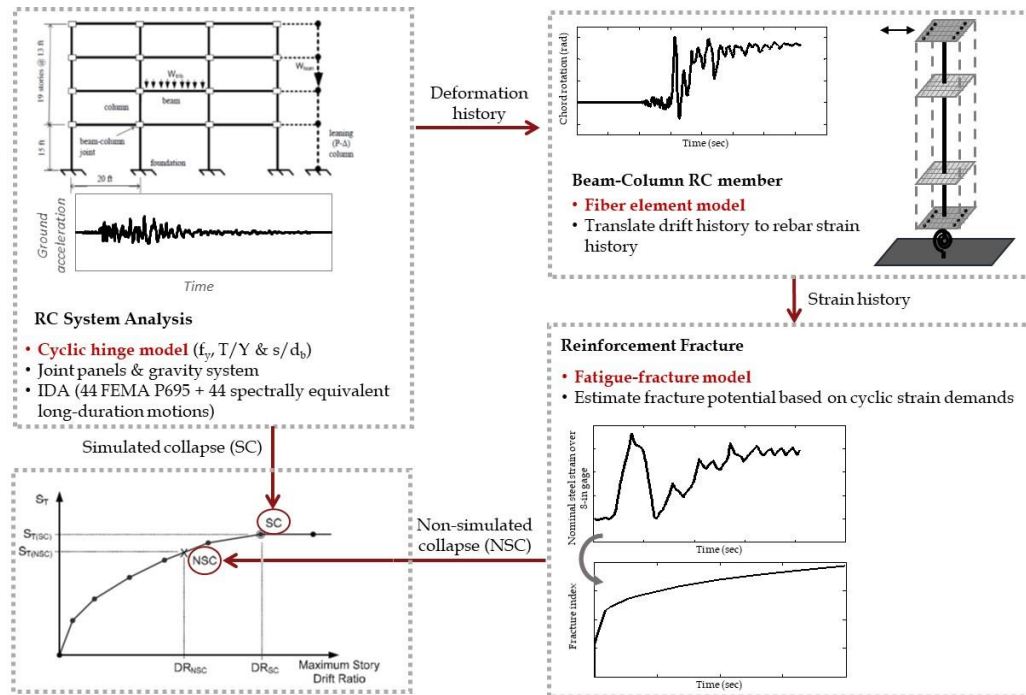


Fig. 6 – Extending FEMA P-695 seismic performance assessment methodology to include the non-simulated collapse mode caused by premature longitudinal reinforcement fractures.

5. Seismic Performance of Special Moment Frames with High-Strength Reinforcement

Following the seismic performance assessment framework introduced in the last section, the influence of high-strength reinforcement on the seismic performance of concrete special moment frames is discussed in this section. One archetype 20-story frame is selected to represent general design practices of the reinforced concrete special moment frames in the US. The original frame is previously examined by the FEMA P-695 study (identified as frame ID 1020). The design of this archetype frame represents mid-rise longer-period buildings jointly controlled by drift (minimum stiffness) and minimum base shear (strength) requirements of ASCE 7 [22]. Given the original frame used Grade 60 reinforcement [23], it is redesigned in this study by using Grade 80 and Grade 100 reinforcement to maintain the same nominal flexural member strengths (M_n). In order to systematically estimate the influence from different steel hardening properties and lateral confinement spacing ratios, overall 27 alternative designs are created with different combinations of T/Y and s/d_b . For Grade 60 steel, T/Y is taken as 1.3, 1.4, or 1.5; for Grade 80 steel, T/Y is taken as 1.2, 1.3, or 1.4; and for Grade 100 steel, T/Y is taken as 1.1, 1.2, and 1.3. Three considered tie spacing ratios are 4, 5, and 6 (the current maximum allowable s/d_b for conventional reinforcement in the concrete special moment frames). Among these 27 design cases, the design using Grade 60 reinforcement with $T/Y = 1.3$ and $s/d_b = 6$ (the minimum requirements by the prevailing design codes) is selected as the benchmark to be compared with.



Utilizing the introduced procedure of evaluating the hinge properties of the IMK model, these frames are idealized to 2D hinge-based models in OpenSees. Based on the modal analysis results, the fundamental period of the frame using high-strength reinforcement is found to be longer than the fundamental period of the frame using Grade 60 reinforcement. The 20-story frame with Grade 60 reinforcement has the first modal period of 2.67s, while the alternative designs with Grade 80 and Grade 100 reinforcement have the first modal periods of 2.95s and 3.20s, respectively. This is mainly because the cross sections using the high-strength reinforcement have relatively lower reinforcement ratios, and thus they have smaller flexural modulus. Related to this stiffness reduction, it is found that the maximum story drift ratios (SDR_{max}) under MCE_R of the frames using Grade 80 and Grade 100 reinforcement are typically 5% and 10% higher than the SDR_{max} under MCE_R of the frames using Grade 60 reinforcement, respectively. The same trend is also observed in a previous study where the increase of drift demand of buildings using Grade 100 reinforcement is reasoned to be caused by the reduced cracked-section stiffness [5]. However, it is noted by the authors that this difference in SDR_{max} demands would be less prominent if the structure with high-strength reinforcement is redesigned to achieve equivalent section stiffness.

Fig. 7a shows the FI_{max} versus SDR_{max} from each analysis for the benchmark frame. Due to the record-to-record uncertainty, the FI_{max} values given a specific SDR_{max} are various under different ground motions. But the median FI_{max} value keeps consistently increasing as the SDR_{max} increases. Referring to Fig. 2c, a larger FI_{max} value indicates a higher bar fracture probability. So, using the median FI_{max} value as a proxy of the bar fracture probability in the structure, we would desire that the median FI_{max} value of the frames with high-strength reinforcement should be comparable to the median FI_{max} value of the benchmark frame. Fig. 7b contrasts the median FI_{max} - SDR_{max} relationships of the frames using Grade 80 reinforcement with the median FI_{max} - SDR_{max} relationship of the benchmark. It is found that the high-strength reinforcement may have smaller fracture probabilities under small drift ratios (e.g., less than 1.5% drift ratio), which is mainly due to the larger yield strains of higher-grade reinforcement. Meanwhile, it is found that the increasing rate of FI_{max} value is much faster in frames using high-strength reinforcement. In the frames using Grade 80 bars with T/Y of 1.4 or Grade 80 bars with T/Y of 1.3 and s/d_b of 5 or smaller, the median FI_{max} values are lower or comparable to the median FI_{max} value of the benchmark design. In the frames using Grade 80 bars with T/Y less than 1.3 or s/d_b greater than 5, the median FI_{max} values are higher than the median FI_{max} in the benchmark design under $SDR_{max} > 3\%$.

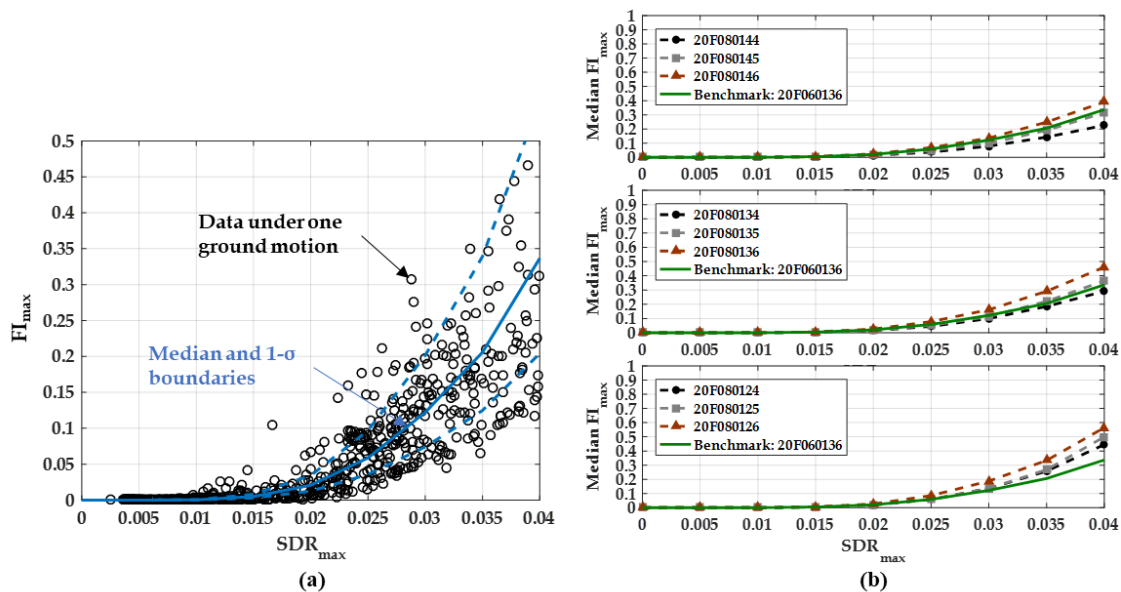


Fig. 7 – FI_{max} - SDR_{max} in the 20-story frames. (a) FI_{max} of the benchmark frame. (b) Median FI_{max} - SDR_{max} of the benchmark frame and the frames using Grade 80 reinforcement.



The introduced assessment framework (Fig. 6) is used to estimate the collapse fragilities with and without reinforcement fracture. To simplify the comparison, the period-dependent ductility ratio and the spectral shape factor are fixed at 5.60 and 1.49 for 20-story frames [20]. Considering record-to-record and modeling uncertainties in the estimated collapse fragility, the dispersion of the fragility function is fixed at 0.5 in this study. Fig. 8a shows three different collapse fragilities of the benchmark design: (1) total collapse probability, (2) non-fracture collapse probability, and (3) fracture-induced collapse probability. In general, after including fracture-induced failures, the median collapse capacity reduces by 2% to 8% [19]. The total collapse fragility is dependent on steel grade, T/Y , and s/d_b with two observed trends in general. First, as shown in Fig. 8b, increasing the T/Y of reinforcing steel increases the median collapse capacity of the frame using high-strength reinforcement. Second, as shown in Fig. 8c, reducing the s/d_b in design also increases the median collapse capacity.

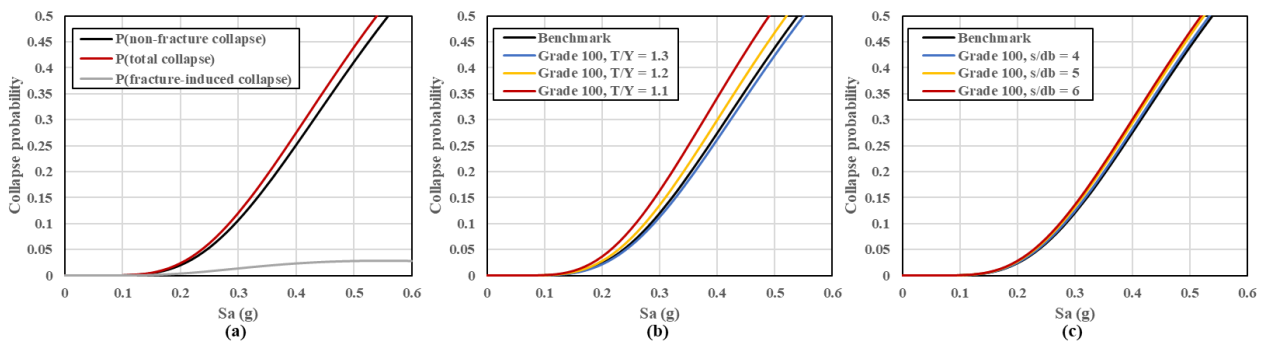


Fig. 8 – Example collapse fragilities based on extended FEMA P-695 assessment framework. (a) Collapse fragilities of the benchmark frame. (b) Influence of T/Y on collapse fragility of frames using Grade 100 bars with $s/d_b = 6$. (c) Influence of s/d_b on collapse fragility of frames using Grade 100 $T/Y = 1.2$ bars.

In practices, the collapse probability at the MCE_R intensity level is used to calibrate the collapse safety of the building [22]. Fig. 9 summarizes the MCE_R collapse probabilities of the 27 archetype frames, where the MCE_R intensity S_a (T_1) is 0.27g. Furthermore, the total collapse probability of each frame is decomposed to the probabilities of collapse with and without bar fracture. On average, bar fracture increases the MCE_R collapse probability by about 0.9% in the benchmark (5.9% to 6.8%), 1.2% in the Grade 80 frames (6.0% to 7.2%), and 1.4% in the Grade 100 frames (7.6% to 9.0%) under MCE_R . It is noted that looser spacings can slightly reduce the collapse capacity, but the collapse probability increases mainly due to decreasing T/Y and increasing steel grade whose combined effects are (1) reduced lateral stiffness; (2) less strain hardening, leading to more strain concentration; and (c) lower cyclic toughness. Moreover, if presuming two limits: (1) T/Y of 1.2 or higher and (2) s/d_b of 5 or less, the probabilities of collapse under MCE_R intensity for the 20-story frames are essentially comparable, i.e., 8%, 9% and 9% for the Grade 60, 80, and 100 frames, respectively. Although the collapse probabilities are larger for the frames with higher grade (lower T/Y and fracture toughness) reinforcement, all of them are within the 10% MCE_R collapse risk limit specified in ASCE 7. The bar fracture risk contributes about 1% to 2% (absolute value) of these collapse probabilities. Meanwhile, without the limits of T/Y and s/d_b , the collapse risks for the Grade 100 frame would increase to 11% (as compared to the 8% and 9% probabilities with the limits imposed), with a larger contribution (up to 3%) from fracture.

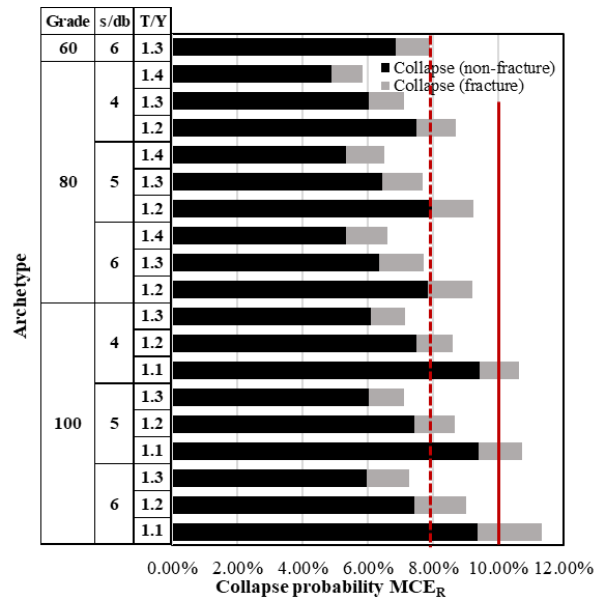


Fig. 9 - Collapse probability of designs of 20-story frames without and with fracture under MCE_R .

6. Conclusion

Based on the available monotonic tensile and cyclic test data of high-strength and conventional reinforcement [3], a parametric reinforcement fatigue-fracture model is developed in this study, which is calibrated and validated to be capable of capturing the reinforcement fracture failures in cyclic-fatigue and concrete subassembly tests. The cyclic deterioration factor in the beam-column hinge model is re-calibrated including new test data to reliably simulate the influence of high-strength reinforcing steel properties. The reinforcement fatigue-fracture is considered as a non-simulated failure mode and incorporated in the collapse assessment by extending the FEMA P-695 methodology.

Following the proposed framework, overall 27 designs of the 20-story archetype special moment frame are designed and analyzed through the IDA approach to investigate the influence of high-strength reinforcement on seismic performance of concrete special moment frames. Reinforcing bar properties and design parameters are considered by parametrically varying reinforcing bar yield strength (f_y) and tensile-to-yield strength ratio (T/Y) and longitudinal bar slenderness (through tie spacing to bar diameter, s/d_b). Based on reported reinforcing bar properties, three T/Y values are considered for each steel grade (1.3, 1.4, and 1.5 for Grade 60; 1.2, 1.3, and 1.4 for Grade 80; 1.1, 1.2, 1.3 for Grade 100). Three s/d_b values (4, 5, and 6) are considered for each type of steel. The following is a summary of the major observations:

1. Reinforcement fracture risk: Referring Fig. 2c, the median FI_{max} is used as a proxy of bar fracture risk at a given SDR_{max} . Two general trends are observed: (1) a larger T/Y results in a lower bar fracture risk at a given SDR_{max} ; and (2) a smaller s/d_b results in a lower bar fracture risk at a given SDR_{max} . Meanwhile, under relatively small story drift ratios ($SDR_{max} < 2\%$), the frames using Grade 80 reinforcement show competitive performance to the benchmark frame. Provided the ACI-318-19 requirements on minimum T/Y to 1.25 and maximum s/d_b to 5.0, the frames using Grade 80 reinforcement have comparable fracture risks to the benchmark if targeting at the maximum allowable SDR_{max} of 4%.

2. Collapse risk (FEMA P-695): As illustrated in Fig. 9, similar to the trends observed for reinforcement fracture, the collapse risk under MCE_R ground motions generally tends to increase for Grade 80, but the increases are more systematically correlated with decreasing T/Y . Reinforcing bar fracture contributes relatively little to the collapse risk. Similar to the point made in regard to bar fracture, parity with the benchmark case with conventional grade steel can be achieved by limiting T/Y to 1.25 and the



maximum tie spacing to $5d_b$. Assuming these limits, the probabilities of collapse at MCE_R are well within the 10% MCE_R collapse risk limit specified in ASCE 7.

3. Grade 100 reinforcement: As illustrated in Fig. 8 and Fig. 9, if conform to the same requirements by the ACI 318-19, the frames using Grade 100 reinforcement also have the acceptable bar fracture risk and the collapse probability at MCE_R , which are also comparable to the bar fracture risk and the collapse probability at MCE_R of the benchmark design.

7. Acknowledgements

This study is made possible by funding from the Charles Pankow Foundation, the Concrete Reinforcing Steel Institute, and ACI's Concrete Research Council. The Project benefited greatly from the Industry Advisory Panel members Dominic Kelly (SGH, Boston) and Ron Klemencic (MKA, Seattle) as well as research collaborators Dr. Jack Moehle, University of California, Berkeley and his graduate student Dr. Duy V. To; and Dr. Wassim Ghannoum, University of Texas, San Antonio and his graduate students Dr. Drit Sokoli, Albert Limantono, Chase Slavin, and Stephen Zhao; and Dr. Andres Lépage and Dr. Rémy Lequesne, University of Kansas and their graduate students Mohammad Huq, Alexander Weber-Kamin, and Shahedreen Ameen. Computing resources are provided by the Blume Earthquake Engineering Center and Sherlock computing cluster at Stanford University.

8. Copyrights

17WCEE-IAEE 2020 reserves the copyright for the published proceedings. Authors will have the right to use content of the published paper in part or in full for their own work. Authors who use previously published data and illustrations must acknowledge the source in the figure captions.

9. References

- [1] National Institute of Standards and Technology. (2014). Use of high-strength reinforcement in earthquake-resistant concrete structures[M].
- [2] Applied Technology Council. (2014). Roadmap for the use of high-strength reinforcement in reinforced concrete design[M]. US Department of Homeland Security, FEMA.
- [3] Slavin C M, Ghannoum W M. (2015). Defining structurally acceptable properties of high-strength steel bars through material and column testing – Part I: material testing report[R]. Charles Pankow Foundation.
- [4] To D V, Moehle J P. (2017). Seismic performance characterization of beams with high-strength reinforcement[R]. Charles Pankow Foundation.
- [5] Sokoli D, Limantono A, Ghannoum W M. (2017). Defining structurally acceptable properties of high-strength steel bars through material and column testing – Part II: column testing report[R]. Charles Pankow Foundation.
- [6] American Concrete Institute. (2019). Building code requirements for structural concrete: ACI 318-19[M].
- [7] Ibarra L F, Medina R A, Krawinkler H. (2005). Hysteretic models that incorporate strength and stiffness deterioration[J]. Earthquake engineering & structural dynamics, 34(12): 1489-1511.
- [8] Mazzoni S, McKenna F, Scott M H, et al. (2006). OpenSees command language manual[J]. Pacific Earthquake Engineering Research (PEER) Center, 264.
- [9] Vamvatsikos D, Cornell C A. (2002). Incremental dynamic analysis[J]. Earthquake Engineering & Structural Dynamics, 31(3), 491-514.
- [10] Applied Technology Council. (2009). Quantification of building seismic performance factors[M]. US Department of Homeland Security, FEMA.
- [11] Miner M A. (1945). Cumulative damage in fatigue journal of applied mechanics 12 (1945) No. 3, pp[J]. A159-A164.



- [12] Manson S S. (1965). Fatigue- a complex subject - some simple approximations[R]. NASA-TM-X-52084. National Aeronautics and Space Administration Cleveland Oh Lewis Research Center.
- [13] Coffin Jr L F. (1954). A study of the effects of cyclic thermal stresses on a ductile metal[J]. Transactions of the American Society of Mechanical Engineers, New York, 76: 931-950.
- [14] Smith R W, Hirschberg M H, Manson S S. (1963). Fatigue behavior of materials under strain cycling in low and intermediate life range[R]. National Aeronautics and Space Administration Cleveland Oh Lewis Research Center.
- [15] Mander J B, Panthaki F D, Kasalanati A. (1994). Low-cycle fatigue behavior of reinforcing steel[J]. Journal of Materials in Civil Engineering, 6(4): 453-468.
- [16] Brown J, Kunnath S K. (2000). Low-cycle fatigue behavior of longitudinal reinforcement in reinforced concrete bridge columns[J].
- [17] Downing S D, Socie D F. (1982). Simple rainflow counting algorithms[J]. International journal of fatigue, 4(1): 31-40.
- [18] Huq M S, Weber-Kamin A S, Ameen S, Lequesne R D, Lepage A. (2017). High-strength steel bars in reinforced concrete walls: influence of steel mechanical properties on deformation capacity[R]. Charles Pankow Foundation.
- [19] Zhong K, Deierlein G G. (2019) Low-cycle fatigue effects on the seismic performance of concrete frame and wall systems with high strength reinforcing steel[R]. Charles Pankow Foundation.
- [20] Haselton C B, Liel A B, Dean B S, et al. (2007). Seismic collapse safety and behavior of modern reinforced concrete moment frame buildings[M]//Structural engineering research frontiers. 2007: 1-14.
- [21] Haselton C B, Liel A B, Taylor-Lange S C, Deierlein G G. (2016). Calibration of model to simulate response of reinforced concrete beam-columns to collapse[J], ACI Structural Journal. Nov/Dec2016, Vol. 113 Issue 6, p1141-1152.
- [22] American Society of Civil Engineers. (2017). Minimum design loads and associated criteria for buildings and other structures: ASCE/SEI 7-16[M].
- [23] Haselton C B. (2008). Beam-column element model calibrated for predicting flexural response leading to global collapse of RC frame buildings[R]. Pacific Earthquake Engineering Research Center.